

# ESP-NOW Performance in Outdoor Environments: Field Experiments and Analysis

Benjamin Becker\*, Christian Oberli†, Julian Zobel\*,  
Ralf Steinmetz\* and Tobias Meuser\*

\*Multimedia Communications Lab (KOM), Department of Electrical Engineering and Information Technology,  
Technical University of Darmstadt, Darmstadt, Germany  
(e-mail: Benjamin.Becker@kom.tu-darmstadt.de, Julian.Zobel@kom.tu-darmstadt.de,  
Tobias.Meuser@kom.tu-darmstadt.de, Ralf.Steinmetz@kom.tu-darmstadt.de)

†Department of Electrical Engineering, Pontificia Universidad Católica de Chile, Santiago, Chile  
(e-mail: obe@uc.cl)

**Abstract**—The Internet of Things plays a crucial role in various fields, such as smart homes, agriculture, and natural disaster prediction. Data typically needs to be transmitted wirelessly to base stations, with each application having its individual Quality of Service requirements. In this work, we provide a better understanding of the functioning of ESP-NOW at the lower layers and the resulting performance of the protocol under real-world conditions. For this, we conduct experiments under controlled conditions with the widely used Heltec WiFi LoRa 32 V3 board. We further conduct experiments in two typical outdoor environments to assess performance under real-world conditions: farmland under line-of-sight conditions with measurements taken at 21 positions and a forest environment with measurements taken at 205 positions. Special emphasis is placed on the packet delivery ratio and the distribution of delays. Finally, we demonstrate that the delay distributions from the outdoor experiments match a model derived from our experiments on ESP-NOW under controlled conditions.

**Index Terms**—ESP-NOW, Performance, One Way Delay, Field-Study, Modeling.

## I. INTRODUCTION

Measurement, control, and monitoring systems help understanding and optimizing processes in the physical world. The *Internet of Things* (IoT) is crucial in various fields, such as smart homes, agriculture, and natural disaster prediction. Due to their low cost, many of these devices are positioned outdoors in remote locations to gather environmental data. To analyze and utilize this data, it typically needs to be transmitted wirelessly to base stations, with each application having its individual Quality of Service requirements. In many application areas, high delays or data loss can lead to negative consequences. This is especially critical for monitoring and control systems, which often have real-time requirements. A comprehensive understanding of the expected delays and the reliability of the communication network is essential for the proper functioning of such systems.

Various communication technologies and protocols are available, each with distinct properties and behaviors. For example, Bluetooth excels at short-range communications up to 100 m with low power consumption, making it ideal for connecting peripherals to other devices. In contrast, LoRa is

designed for low-power communication over long distances of several kilometers at low data rates.

In this study, we focus on ESP-NOW, a protocol that offers low power consumption and compatibility with low-cost transceivers. While ESP-NOW can work with both WiFi and Bluetooth Low Energy, we exclusively examine its WiFi implementation. It is used in numerous applications in the IoT sector, including fields such as agriculture, industry, and smart homes [1]. ESP-NOW comprises all layers between a native IEEE 802.11-1999 standard physical layer [2] and the application layer. The performance of ESP-NOW has been examined in various studies. Compared to protocols like WiFi and Bluetooth, ESP-NOW has demonstrated high range, low latency, and low energy consumption [1], [3]. However, ESP-NOW offers only limited transparency regarding the details of its operation. Such insights into the behavior of a protocol are essential for modeling system performance, as done in works like [4], and for evaluating its performance and reliability in practical applications.

In this work, we aim to better understand wireless communication in modern delay-critical IoT applications and provide insights for developing and analyzing future wireless microcontroller-based systems. Therefore, we investigate the functioning of the ESP-NOW protocol at lower layers by conducting indoor experiments under controlled conditions. To assess the protocols resulting performance under real-world conditions, we conduct experiments in two typical outdoor environments. In farmland under line-of-sight conditions, we take measurements at 21 different distances, and in a forest environment, we take measurements at 205 positions to capture the one-way delay, jitter, and reliability of devices using ESP-NOW. Based on the insights from the experiments under controlled conditions, our last contribution is a model capable of reconstructing the results of the outdoor experiments. We discuss related research in Section II, followed by a description of the Heltec WiFi LoRa 32 V3 in Section III. Next, in Section IV, we describe the ESP-NOW protocol and present experiments conducted under controlled conditions to investigate its functioning. The methodologies for the outdoor experiments are presented in Section V, and the evaluation of

the results in Section VI focuses particularly on the *Packet Delivery Ratio* (PDR) and the distribution of link delays. In Section VII, we propose a model, which we validate using the experiment results from Section VI.

## II. LITERATURE REVIEW

The performance of ESP-NOW has already been evaluated in various studies in the past and compared with other protocols, whereby a wide variety of framework conditions were considered. In all of the following studies, the default settings of the respective protocols were used.

Several studies analyzed the range of ESP-NOW in residential areas under lines-of-sight conditions. Sources report ranges of 190 m [5] and 220 m [6] with ESP32 boards. In [7], up to 250 m were achieved with ESP8266 ESP-01 modules.

In [3], three protocols were compared under identical conditions on ESP32-CAM development boards. In this study, various aspects, such as range, signal strength and power consumption were considered. Using the built-in antenna, maximum ranges of 15 m for Bluetooth, 84 m for WiFi, and 185 m for ESP-NOW were determined. Latency was measured by directly connecting two development boards via cable. The results show that ESP-NOW achieved significantly lower latency than the other two protocols, with 1059  $\mu$ s for a 1-byte payload and 1869  $\mu$ s for a 100-byte payload.

In [1], an ESP32 WROOM was used to compare ESP-NOW, a proprietary long-range mode of ESP-NOW, and WiFi TCP. They assessed the protocols' performance in terms of range, packet delivery ratio, power consumption, and penetration capability in an indoor environment. This study found that ESP-NOW in this obstacle-rich environment had a better range and lower packet loss rate than a typical WiFi TCP approach. ESP-NOW's long-range mode did not show significant performance improvements.

Khanchuea et al. [8] evaluated the performance of ESP-NOW in a multi-hop network. The use case of building automation in an office environment was considered, examining the effects of distance and the number of hops on the resulting round trip time, throughput, and jitter. The authors concluded that ESP-NOW is a good choice for wireless multi-hop, low-power sensor networks.

Labib et al. [9] compared the performance of ESP-NOW and Bluetooth Low Energy in a series of indoor and outdoor experiments. They determined a 15 m indoor and 90 m outdoor range for ESP-NOW and concluded that ESP-NOW achieves up to 15 times the range of Bluetooth Low Energy.

ESP-NOW has been compared to other protocols and technologies in numerous studies. Many of these studies highlight different performance aspects in various environments. Regarding average latency, energy consumption, and range, ESP-NOW has demonstrated good performance in all comparisons, making it very attractive for IoT applications.

However, all of the mentioned works focused on metrics, such as maximum range, transmission rate, PDR, bitrate, or received signal strength. Such metrics work well to describe links in environments with stable and predictable transmission

conditions. Previous work measures delays under controlled laboratory conditions without considering real-world scenarios. However, in challenging environments with significant delay variations and low PDR, aspects such as reliability and delay distributions might be more suitable for a deeper evaluation. Therefore, we analyze the protocol under *realistic, reproducible conditions* to provide more accurate insights. Further, insights into the mechanisms of ESP-NOW are needed to interpret the results.

## III. HELTEC WiFi LoRa 32 V3

The Heltec WiFi LoRa 32 V3 is an IoT development board crafted and manufactured by Heltec Automation [10]. This device is equipped with an ESP32-S3 MCU and features various memory resources, including 384 KB ROM, 512 KB SRAM, 16 KB RTC SRAM, and 8 MB SiP Flash. The SRAM memory was used during our experiments for direct storage of measurement results. The board is powered by a 3.7 V lithium battery, enabling flexible deployment in diverse experimental environments. For wireless connectivity, the board supports WiFi 802.11 b/g/n standards with speeds of up to 150 Mbps and comes with a 2.4 GHz spring antenna. It has a maximum TX power of  $21 \pm 1$  dBm and a receiving sensitivity of  $-136$  dBm. Additionally, the board includes an integrated OLED display, which allowed for status monitoring during our experiments. With a total of 38 pins, the Heltec WiFi LoRa 32 provides multiple connectivity options for integrating various peripherals and sensors. The device also features a Type-C USB interface for data transfer and uses a high-precision temperature-compensated crystal oscillator for stable timing. This crystal oscillator played a central role in our experiments, as it enabled precise measurements of delays.

In summary, the Heltec WiFi LoRa 32 V3 offers a range of features and connectivity options suitable for our experiments measuring delays and packet loss ratios of ESP-NOW.

## IV. ESP-NOW PROTOCOL

ESP-NOW is a connectionless wireless communication protocol developed by Espressif [11]. ESP-NOW offers a high adoption within the IoT community, coupled with its ability to provide low latencies at relatively low energy consumption [3]. It is based on the data-link layer and can work with WiFi and Bluetooth LE. When working with WiFi, all ESP-NOW traffic uses exclusively WiFi action frames. ESP-NOW facilitates low-power transmission of small messages containing payloads of up to 250 bytes between interconnected ESP32 or ESP8266 boards. It supports both encrypted and unencrypted unicast communication as well as unencrypted broadcasts. All experiments in this work were conducted using the standard configuration of ESP-NOW provided by ESP-IDF version 4.4.6.

The low-level mechanisms of ESP-NOW have been scarcely investigated beyond the official specifications provided by Espressif. In a blog post published in 2018, it was experimentally determined that packets are sent multiple times with

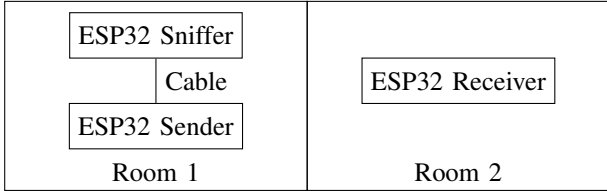


Figure 1. Experimental setup for investigating low-level behavior of ESP-NOW.

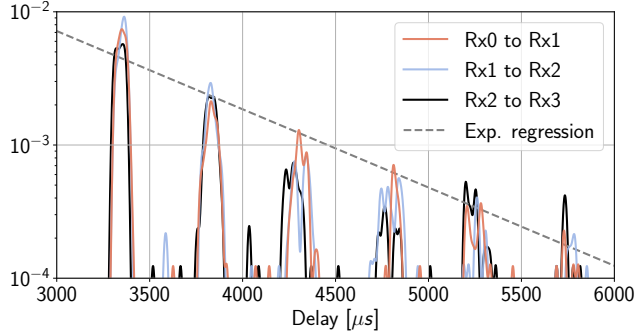


Figure 2. Distribution of time intervals between reception of retransmissions using ESP-NOW.

a decreasing data rate [12]. In [1] the authors state that ESP-NOW uses the default IEEE 802.11 CSMA mechanism, with the number of retransmissions set to 10 by default.

To gain up-to-date insights into the behavior of this ESP-NOW version, we conducted a set of experiments under controlled conditions. In these experiments, one ESP32 device continuously sends packets with a payload of 250 bytes to a second ESP32 device. Both devices are placed in different rooms. Each transmitted packet contains a unique identifier, allowing the identification and tracking of retransmissions. A third device, a WiFi Sniffer, is positioned next to the Sender node to detect transmissions. Sniffer and Sender nodes are interconnected via the GPIO pins. Whenever starting a transmission, the sender sends a HIGH signal, allowing a precise delay measurement for message reception at the sniffer using its internal high-precision clock. The setup is shown in Figure 1. By retrospectively filtering data based on the traffic registered by the Sniffer, we can largely rule out interferences at the Sender node in the final dataset.

We first measured the time intervals between passing the frame to ESP-NOW for transmission at the Sender side and receiving the first transmission at the Sniffer. All measured time intervals ranged from  $2673 \mu s$  to  $2780 \mu s$ , a timespan of  $107 \mu s$ .

The graphs in Figure 2 show the distributions of the time intervals between reception of the initial transmission and reception of the first retransmission (Rx0 to Rx1), between the first retransmission and second retransmission (Rx1 to Rx2), and between the second retransmission and third retransmission (Rx2 to Rx3). Each graph represents data from 5000 measurements. A Gaussian filter with a standard deviation of  $10 \mu s$  has been applied to improve visual clarity. The

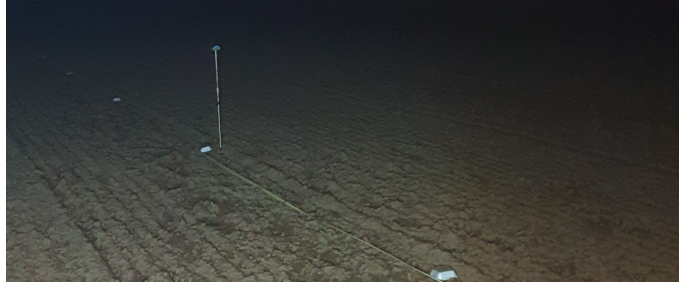


Figure 3. The farmland experiments were conducted in a flat terrain devoid of vegetation or obstacles.

exponential regression of all local maxima greater than  $10^{-4}$  has been calculated and is shown as a dashed line.

The graphs clearly show spikes with diminishing height and exhibit characteristics resembling a geometric distribution. This indicates the presence of a p-persistent IEEE 802.11 protocol, which only differs from the standard protocol in the backoff interval, which is sampled from a geometric distribution [13]. The presence of spikes also indicates the use of timeslots, with an average interval of  $481 \mu s$ . The first spike starts at  $3373 \mu s$  and ends at  $3480 \mu s$ .

We observed that all transmitted packets used the IEEE 802.11b WiFi version at the default data rate of  $1 Mbit/s$  and a channel bandwidth of  $20 MHz$ . Additionally, we detected up to 31 retransmissions of packets.

## V. OUTDOOR EXPERIMENT METHODOLOGY

To measure ESP-NOW performance under realistic conditions, we designed an extensive outdoor experiment setup focusing on delay measurements.

The experiment conditions were carefully chosen to minimize the influence of external factors. The experiments were conducted in farmland (GPS-location:  $49.876993, 8.55979$ ) and a forest (GPS-location:  $49.869273, 8.610231$ ), exclusively at nighttime to minimize disturbances. The weather remained dry throughout all experiments, with temperatures between  $4^\circ C$  and  $6^\circ C$ . No nearby WiFi access points could be detected. The person conducting the experiments also maintained a distance of at least  $5 m$  from all devices during the experiments, with his mobile phone in flight mode. No other humans or animals were noted during the experiments.

The open farmland location featured flat terrain, devoid of vegetation or obstacles, as shown in Figure 3. This location facilitated unobstructed communication with no shadowing. The forest provided a more diverse environment, with rich vegetation and uneven ground. Canopies and foliage on the ground can significantly influence the propagation of wireless signals by reflecting them, while tree trunks absorb electromagnetic waves [14]. Scattering and small scale fading in the forests can be relatively severe [15]. The location within the forest was deliberately selected to feature a single line-of-sight path with a length of  $65 m$ . To ensure line-of-sight conditions, a string was stretched at a height of  $1 m$ , starting from the Sender node, as shown in Figure 4. The string further eased



Figure 4. In the forest experiments, a green string was stretched at a height of 1 m to ensure line-of-sight communication. A red light source is visible over a distance of 65 m.

measuring the Receiver node's positions, which was placed at 205 different positions in a  $40\text{ m} \times 5\text{ m}$  grid, with a minimum distance of 25 m and a maximum distance of 65 m from the Sender.

#### A. Hardware for Outdoor Experiments

The outdoor experiments employed three sets of identical hardware, each comprising a Heltec WiFi LoRa 32 board, a battery pack, an aluminum monopod measuring 0.95 m, and a plastic casing. The low antenna height was selected because sensors in forest environments are typically mounted below 2 m [15]. The deliberate choice of limited hardware aimed to reduce potential interference factors and enhance the replicability of the experiments. The ESP32 boards were mounted on a monopod in plastic casings to shield the devices from humidity and other external stresses.

To monitor the experiments and better interpret the results, we positioned a Wi-Fi sniffer at a distance of 5 meters from the transmitter. This node does not send any data itself and is solely responsible for monitoring the experiments. It records all detected transmissions during the experiment, along with their associated metadata.

#### B. Delay Measurement

Measuring the one-way delays between sending and receiving a message can be approached in various ways. Connecting the devices via cable, e.g., as described in Section IV and [3], provides precise measurements. It is, however, impractical for long distances in uneven terrain. GPS transmitters can provide time synchronization, typically with an accuracy of a few microseconds. The accuracy depends on several factors, including the quality of the GPS module, the strength of the GPS signal, and environmental conditions.

A plethora of clock synchronization protocols have been developed in the past decades [16], [17]. Many clock synchronization protocols are based on the assumption of symmetrical link delays from one node to another and back. This assumption, however, does not hold in general, especially in challenging environments. Also, random waiting periods before transmissions, as utilized in IEEE 802.11b, inherently render this synchronization procedure inaccurate. Without direct access to the MAC layer, these uncertainties can lead to inaccurately synchronized clocks.

For our study, we opted for *Reference Broadcast Synchronization* (RBS) [18], which provides accurate synchronization using wireless communication [17]. A dedicated synchronization node broadcasts a message, which other nodes use to synchronize their clocks. This approach eliminates uncertainty inherent in traditional time synchronization protocols, as non-deterministic delay in wireless transmission mainly occurs between packet construction and transmission.

We modified RBS to increase its accuracy. To reduce skew, the synchronization node repeatedly broadcasts its current timestamp during a synchronization phase. The other devices update their logical clocks only if the overheard timestamp is smaller than the current logical time of that node. The effects of clock drift are minimized by repeating the procedure after each experiment. The synchronization node is positioned equidistantly between the two other devices, and synchronization is considered successful only if at least 95% of the synchronization messages are successfully received by both other nodes. We measured the accuracy of the modified RBS via a dedicated cable between two devices and consistently achieved a clock difference below one microsecond.

Measuring one-way delays during the experiments is based on the synchronized clocks. The Sender node timestamps packets before passing them to ESP-NOW for transmission, and the Receiver node then measures the packet delays upon reception. To avoid queuing delays, packets are sent only after successfully transmitting a previous packet.

#### C. Experiment Phases

Each experiment lasts 32 s, where a small proportion of time is used for clock synchronization and ensuring that all devices are ready. The experiment is split into the following phases:

**Clock synchronization:** The clocks of Sender and Receiver are synchronized using the modified RBS.

**Confirmation:** Sender and Receiver confirm a successful synchronization process.

**Start Signal:** If clock synchronization is successful, the synchronization node sends a start signal for the experiments.

**Experiment:** The Sender unicasts 500 messages, each with a 250-byte payload, to the Receiver for delay measurement.

**Collect data:** The Receiver broadcasts the results of the experiments for monitoring and logging purposes.

**Reset:** All nodes return to the Clock synchronization phase.

## VI. RESULTS AND ANALYSIS

To assess the performance of the wireless communication using ESP-NOW in the farmland and forest experiments, respectively, we examine the *Packet Delivery Ratio* (PDR) and jitter. PDR is measured as the ratio of successfully received packets to the number of transmitted packets, and jitter is measured as the standard deviations of the delays.

#### A. Performance in the Open Farmland

Figure 5 presents the PDR on the y-axis and the distance on the x-axis. Larger distances up to 90 m were tested but are not displayed on the graph, as no packets were received.

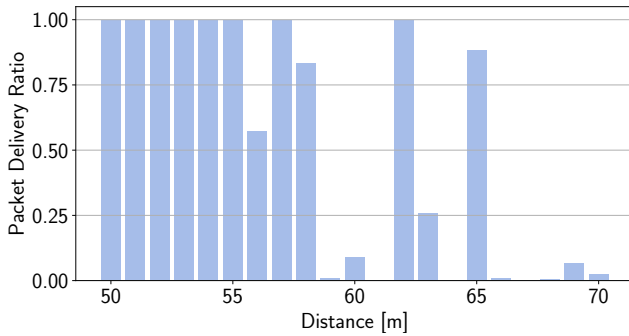


Figure 5. PDR at different distances on farmland.

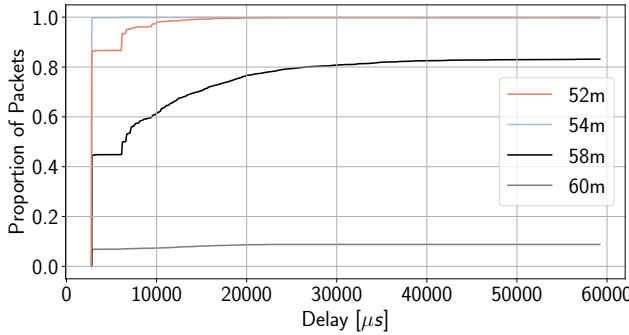


Figure 6. Empirical delay distributions at different distances on the farmland.

Below 55 m, 99.97% of packets were received correctly. Above 55 m, the PDR does not decrease continuously with increasing distance, contrary to the expected behavior according to the two-way ground reflection model. Instead, the links exhibit a high PDR at certain distances, such as 62 m and 65 m. Conversely, the link PDR drops to zero at other distances, such as 59 m, 61 m, and 64 m.

To explain the low PDR around 60 m, we analyzed the data from the Wi-Fi sniffer. We observed that all transmissions from the Sender were 802.11b/g MPDU packets, transmitted at a data rate of 1 Mbit/s with a 20 MHz channel bandwidth on either channel 0 or channel 1. We also tried to explain the low PDR by using the two-ray ground-reflection model without success. However, during the experiments, we noticed that even small changes in the position or orientation of the receiver lead to significant variations in link quality. This could be attributed to the antenna heights of 95 cm, as the Fresnel zone was not entirely free of obstructions.

Figure 6 illustrates four representative *empirical cumulative distribution functions* (ECDFs) of the delays measured at specific distances. The x-axis shows the delay in microseconds, ranging from 0  $\mu$ s to 60000  $\mu$ s, and the y-axis shows the ratio of packets that experienced a delay below that particular delay.

The graph for the distance of 54 m exhibits an almost constant delay with an average of 2782.85  $\mu$ s, a standard deviation of 108.72  $\mu$ s and a maximum PDR of 1, which also indicates that no interference affected the experiments.

Another link with good performance is the one at a distance of 52 m. It achieves a PDR of 99.85%, an average delay of

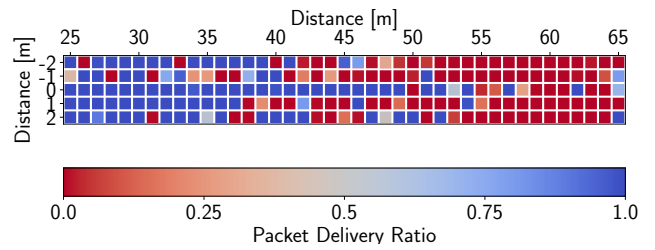


Figure 7. PDR at different receiver positions in forest.

3461.65  $\mu$ s, and a standard deviation of 2079.06  $\mu$ s. 86.65% of packets are delivered within the first 3120  $\mu$ s. The graph then shows a horizontal segment from 2840  $\mu$ s to 6070  $\mu$ s. No packets were successfully delivered with those delays. This can be explained by the mechanisms of the ESP-NOW protocol, which starts the initial transmission of packets under clear channel conditions almost immediately, as observed in Section IV. The y-offset of the horizontal segment represents the probability of successful first transmission. After 6070  $\mu$ s, the graph exhibits an interesting curve. The graph eventually reaches its maximum at 25628  $\mu$ s.

At a distance of 58 m, a PDR of 83.2% was achieved, at an average delay of 7851.15  $\mu$ s with a standard deviation of 8033.23  $\mu$ s. The first transmission had a success rate of 44.85%. Following a horizontal segment between 2840  $\mu$ s and 6070  $\mu$ s, a composition of multiple small curves is recognizable, similar to the ones in the graph observed for the 52 m distance. The graph eventually reaches its maximum at 59192  $\mu$ s.

At a distance of 60 m, a PDR of 8.9% was achieved, at an average delay of 5196.42  $\mu$ s with a standard deviation of 4935.95  $\mu$ s. The first 6144  $\mu$ s are as expected for a link with bad quality, showing a success rate of 6.9% for the first transmission. However, the remainder of the graph suggests low success rates for retransmissions.

The results from these experiments exhibit a variety of ESP-NOW links with different characteristics at different distances. Even in an empty farmland without any obstacles or interference, distance alone is insufficient to determine the performance of these links. The findings underscore the challenges in predicting and explaining the performance of ESP-NOW. However, the curves fit the observations in Section IV.

### B. Performance in the Forest

In the following analysis, we focus on the performance at the different measurement points in the forest environment. All ECDFs obtained from those experiments are similar to those presented in Section VI-A and, therefore, not shown.

In addition to the previous experiments with pure line-of-sight, we shifted the receiver device up to 2 m left and right, perpendicular to the drawn string. This offset is represented in Figure 7 on the y-axis, the color-coded squares indicate the PDR at each measurement point. Out of the 205 measurement positions, 133 provided links with a PDR above zero.

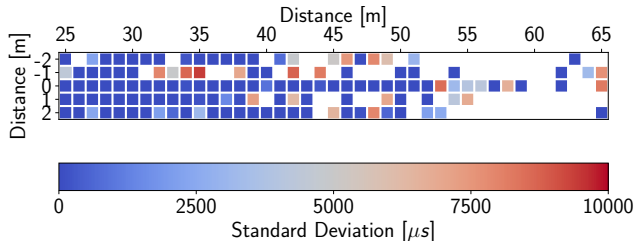


Figure 8. Jitter at different receiver positions in forest.

The line-of-sight path (offset 0) shows a clear similarity to the PDR from the open farmland experiment (cf. Figure 5). The only two distances where the PDR significantly deviates between the two experiments are 50 m and 55 m. While the PDR in the farmland reached 1 at those distances, it is close to zero in the forest. Various environmental factors may cause this deviation, such as the influence of uneven terrain or vegetation.

For the positions that are offset to either side, particularly above 40 m, there are many impaired links with low PDRs, probably due to heavy shadowing caused by large trees. Generally, a decrease in link quality with increasing distance can be observed. However, numerous deviations from this trend exist, similar to what has been reported in related studies [19]. Interestingly, the links in the top left quarter of the measurement region provide a relatively high performance, despite the presence of two large trees obstructing the line of sight. In these cases, the signal penetrates through the trees and/or reaches the Receiver through reflections. In the lower left region, there are mostly links with high PDRs. However, the influence of smaller trees in all regions can neither be confirmed nor ruled out. Notably, for most distances, links with a line-of-sight connection exhibit higher or equal PDR compared to those without a line-of-sight connection. The only exceptions are the links at a distance of 65 m.

In Figure 8, the jitter of the delays is represented by colors. Measurement points with a PDR of zero are indicated by white spaces. The jitter is lowest along the line of sight and generally increases with distance. High jitter can also be observed in the top left quarter of the measurement area, where two large trees obstruct the line of sight.

Jitter and PDR are tested using Spearman and Kendall correlation. The resulting coefficients (p-values) are  $-0.44$  ( $1.56 \times 10^{-7}$ ) for Spearman and  $-0.33$  ( $2.85 \times 10^{-7}$ ) for Kendall, respectively, each indicating a statistically significant negative correlation. Thus, links characterized by high jitter often exhibit a low PDR. However, there are also numerous exceptions to this pattern.

In summary, many links observed in this experiment exhibit low PDRs or significant jitter, indicating pronounced stochastic properties of the links. This is especially true for links ranging over long distances or obstructed by trees. Even minor variations in node positioning can significantly impact link quality and performance. Also, high jitter often correlates with a decreased PDR. Due to the complexity of

the environment and the limited information available on the mechanisms used by ESP-NOW, it is difficult to make definitive statements about the exact reasons for the resulting performance. This emphasizes the importance of conducting field tests to determine genuine real-world link performance.

## VII. MODEL FOR ESP-NOW DELAYS

To contribute to the modeling of delays in real-world environments using ESP-NOW, in this section, we generate a model based on the results from Section IV.

For this, we utilize the probability mass function  $G$  of a geometric distribution with parameter  $p_{\text{per}}$ . For simplicity, we assume  $G$  takes the value 0 for function values outside the natural numbers. The initial transmission is represented by a unit impulse function  $d_0$ . For each retransmission in the model, we compute a function  $d_n$ , where  $n \geq 1$  denotes the  $n$ th retransmission. This function  $d_n$  is calculated as convolution, denoted by  $*$ , of  $d_{n-1}$  with  $G$  as follows:

$$d_n = d_{n-1} * G. \quad (1)$$

We scale the x-axis of the functions  $d_n$  by a factor  $t_{\text{slot}}$  to incorporate the slot duration into the model. Subsequently, we shift the distributions to the rights by  $t_{\text{tx}}$  for the initial transmission delay and  $nt_{\text{rtx}}$  for the delay of retransmissions. The delays are described by the resulting distributions

$$b_n(x) = d_n(x/t_{\text{slot}} - t_{\text{tx}} - nt_{\text{rtx}}). \quad (2)$$

$p_{\text{succ},n}$ , which describes the probability that the  $n$ th (re)transmission is the first successful transmission, is calculated using two parameters. A base value  $p_{\text{phy}}$  describes the success probability of the initial transmission. A factor  $r \leq 1$  is used to decrease the success probability with each failed transmission attempt continuously.

$$p_{\text{succ},n} = p_{\text{phy}} r^n (\prod_{i=0}^{n-1} (1 - p_{\text{phy}} r^i)). \quad (3)$$

The product  $b_n p_{\text{succ},n}$  is, thus, a function that describes the contribution of the  $n$ th retransmission to the overall density function of the delays. The final probability density function  $f$ , which includes the initial transmission and all  $n_{\max}$  retransmissions, is obtained as the sum of these functions:

$$f = \sum_{n=0}^{n_{\max}} b_n p_{\text{succ},n}. \quad (4)$$

The chosen parameters for the model are mostly based on averages of the measurements described in Section IV. The initial transmission delay is set to  $t_{\text{tx}} := 2800 \mu\text{s}$ , the retransmission delay is set to  $t_{\text{rtx}} := 3350 \mu\text{s}$ , the slot duration to  $t_{\text{slot}} := 481 \mu\text{s}$ , and the retransmissions limit to  $n_{\max} := 31$ . The persistence probability  $p_{\text{per}}$  and the factor  $r$  are optimized to minimize the *Mean Squared Error* (MSE) over the first 40 ms, relative to the curves observed in the outdoor experiments. The success probability of the initial transmission  $p_{\text{phy}}$  is set to the value of the experiment curve at 5000  $\mu\text{s}$ .

Four curves generated by our model, aiming to fit the experimental curves shown in Figure 6, are depicted in Figure 9. The MSE and *Mean Absolute Error* (MAE) between the model and experiment results are shown in Table I.

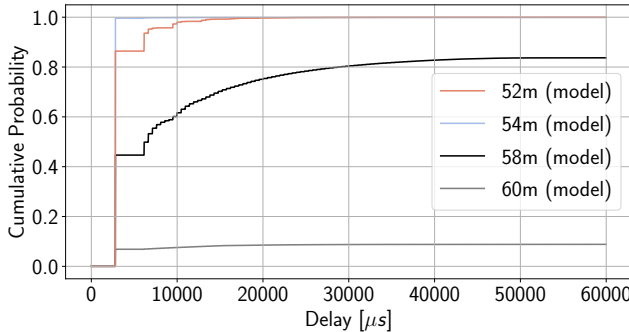


Figure 9. Model-generated delay distributions.

Table I  
DIFFERENCE BETWEEN MODEL AND EXPERIMENTS.

Graph	Mean Absolute Error	Mean Squared Error
52 m	$1.63 \times 10^{-3}$	$2.10 \times 10^{-4}$
54 m	$9.36 \times 10^{-4}$	$3.02 \times 10^{-4}$
58 m	$3.46 \times 10^{-3}$	$7.37 \times 10^{-5}$
60 m	$8.12 \times 10^{-4}$	$4.39 \times 10^{-6}$

Furthermore, all 133 ECDFs from the forest experiments in Section VI-B with a PDR greater than 0 are reconstructed using the model. The model achieved an average MSE of  $1.70 \times 10^{-4}$  and a maximum MSE of  $5.04 \times 10^{-4}$  between the curves. The average MAE is  $1.2 \times 10^{-3}$ , with a maximum MAE of  $1.2 \times 10^{-2}$ . Despite the experimental data stemming from complex environments and the exact mechanisms of ESP-NOW being unknown, the model reconstructs all observed curves with little error. This demonstrates the model's effectiveness in replicating experimental results. Additionally, the small errors further confirm the findings from Section IV regarding the p-persistent backoff mechanism.

### VIII. CONCLUSIONS

In this work, we investigated ESP-NOW and measured its performance. Initial experiments under laboratory conditions were conducted to analyze the protocol behavior since the exact mechanisms of ESP-NOW are unknown. The results clearly indicate a slotted p-persistent channel access mechanism, as present in a p-persistent IEEE 802.11 protocol. Furthermore, we developed a methodology for real-world experiments to measure one-way delays in controlled outdoor environments, utilizing the Heltec WiFi LoRa 32 V3. We conducted two extensive field tests in an open farmland and a forested area, respectively. In total, 246 different positions with different distances between sender and receiver were tested. The experiments revealed that many links exhibit significant jitter and low *Packet Delivery Ratio* (PDR), even in the absence of obstacles, interference, or other disturbances. It was demonstrated that proper positioning of nodes can result in highly reliable links that meet soft real-time requirements. However, evaluating performance in environments with significant radio interference requires further studies. Out of all 153 links with a PDR above 0, a total of 93 had a PDR

above 95% and 106 links had a PDR above 50%. Also, in the open farmland experiment, the PDR was constantly above 99% below 56 m but zero above 70 m. Interestingly, between 56 m and 70 m, the PDR fluctuates between 100% and zero instead of steadily decreasing with higher distance.

We also analyzed the relationship between jitter and PDR, which were shown to be negatively correlated.

Finally, we formulated a model based on our test results of ESP-NOW under controlled conditions. The model successfully reconstructed all delay distributions observed in the outdoor experiments with an average *Mean Absolute Error* of 0.0012, demonstrating the model's effectiveness in replicating experimental results.

However, further adaptations of our model are required to quantify ESP-NOW performance in dynamic and interference-prone settings. Future work therefore encompasses performance measurements in scenarios with demanding channel conditions. For example, urban deployment scenarios will likely yield lower PDR and higher jitter than rural settings due to increased radio interference and reduced signal quality, making urban areas an ideal context for further research. Nonetheless, our model already stands as a tested and valuable means of estimating delay distributions and is usable for researchers for predictive and simulation purposes.

### REFERENCES

- [1] D. Urazayev, A. Eduard, M. Ahsan, and D. Zorbas, "Indoor performance evaluation of esp-now," in *2023 IEEE International Conference on Smart Information Systems and Technologies (SIST)*. IEEE, 2023, pp. 1–6.
- [2] G. R. Hiertz, D. Denteneer, L. Stibor, Y. Zang, X. P. Costa, and B. Walke, "The ieee 802.11 universe," *IEEE Communications Magazine*, vol. 48, no. 1, pp. 62–70, 2010.
- [3] D. Eridani, A. F. Rochim, and F. N. Cesara, "Comparative performance study of esp-now, wi-fi, bluetooth protocols based on range, transmission speed, latency, energy usage and barrier resistance," in *2021 International Seminar on Application for Technology of Information and Communication (iSemantic)*. IEEE, 2021, pp. 322–328.
- [4] B. Becker, C. Oberli, T. Meuser, and R. Steinmetz, "On maximizing the probability of achieving deadlines in communication networks," *Journal of Sensor and Actuator Networks*, vol. 13, no. 1, p. 9, 2024.
- [5] R. Pasic, I. Kuzmanov, and K. Atanasovski, "Esp-now communication protocol with esp32," *Journal of Universal Excellence*, vol. 6, no. 1, pp. 53–60, 2021.
- [6] R. Santos and S. Santos. (2020) Esp-now two-way communication between esp32 boards. Accessed: 7/2024. [Online]. Available: <https://randomnerdtutorials.com/esp-now-two-way-communication-esp32/>
- [7] H. Cheung. (2020) Esp-01 range test with esp-now protocol. Accessed: 7/2024. [Online]. Available: <https://www.e-tinkers.com/2020/05/esp-01-range-test-with-esp-now-protocol/>
- [8] K. Khanchuea and R. Siripokarpirom, "A multi-protocol iot gateway and wifi/ble sensor nodes for smart home and building automation: Design and implementation," in *2019 10th International Conference of Information and Communication Technology for Embedded Systems (IC-ICTES)*. IEEE, 2019, pp. 1–6.
- [9] M. I. Labib, M. ElGazzar, A. Ghalwash, and S. N. AbdulKader, "An efficient networking solution for extending and controlling wireless sensor networks using low-energy technologies," *PeerJ Computer Science*, vol. 7, p. e780, 2021.
- [10] Heltec Automation. (2023) Wifi lora 32 (v3) - heltec automation. Accessed: 3/2024. [Online]. Available: <https://heltec.org/project/wifi-lora-32-v3/>
- [11] Espressif Systems. (2024) Esp-now by espressif systems. Accessed: 7/2024. [Online]. Available: <https://www.espressif.com/en/solutions/low-power-solutions/esp-now>

- [12] T. Flayols. (2018) How esp-now really works. Accessed: 7/2024. [Online]. Available: <https://hackaday.io/project/161896-linux-espnow/log/154698-how-esp-now-really-works>
- [13] F. Cali, M. Conti, and E. Gregori, "Dynamic tuning of the ieee 802.11 protocol to achieve a theoretical throughput limit," *IEEE/ACM Transactions on Networking*, vol. 8, no. 6, pp. 785–799, 2000.
- [14] M. Mutschlechner, P. Baldemaier, P. Handle, and F. Dressler, "Wireless in the woods: Experimental evaluation of ieee 802.11 a/b/g in forested environments," *12. GI/ITG FACHGESPRÄCH SENSORNETZE*, vol. 60, p. 5, 2013.
- [15] D. P. Smith, G. G. Messier, and M. W. Wasson, "Boreal forest low antenna height propagation measurements," *IEEE transactions on antennas and propagation*, vol. 64, no. 9, pp. 4004–4011, 2016.
- [16] I.-K. Rhee, J. Lee, J. Kim, E. Serpedin, and Y.-C. Wu, "Clock synchronization in wireless sensor networks: An overview," *Sensors*, vol. 9, no. 1, pp. 56–85, 2009.
- [17] H. Yiğitler, B. Badihi, and R. Jäntti, "Overview of time synchronization for iot deployments: Clock discipline algorithms and protocols," *Sensors*, vol. 20, no. 20, p. 5928, 2020.
- [18] J. Elson, L. Girod, and D. Estrin, "Fine-grained network time synchronization using reference broadcasts," *ACM SIGOPS Operating Systems Review*, vol. 36, no. SI, pp. 147–163, 2002.
- [19] J. Zobel, P. Frommelt, L. Laufenberg, R. Fayard, L. Wehrstein, R. Kundel, and R. Steinmetz, "Lorameter: Signal mapping in lora networks," in *2023 International Conference on Software, Telecommunications and Computer Networks (SoftCOM)*. IEEE, 2023, pp. 1–6.